PERFORMANCE OF THE REYNOLDS STRESS MODEL IN THE PREDICTION OF THE HEAT TRANSFER OF AN IMPINGING JET

D.I. Maldonado, dimt@aluno.puc-rio.br
A.O. Nieckele, nieckele@puc-rio.br
Department of Mechanical Engineering – Pontifícia Universidade Católica de Rio de Janeiro, PUC/Rio
Rua Marquês de São Vicente, 225 – Gávea, 22453-900, Rio de Janeiro – RJ – Brasil

Abstract. *Impinging jet is an efficient mechanism to enhance wall heat transfer (also mass transfer); therefore, it is widely used in engineering applications. The flow field of an impinging jet presents a complex flow phenomenon, with the presence of a potencial core, stagnation region, shear layer and wall jet. Due to the flow complexity it is an excellent problem to evaluate turbulence models. In the present work, a numerical study was carried out using the finite-volume method. Due to the anisotropic chacacteristics of an impinging jet, the Reynolds Stress Model (RSM) was selected to predict this type of flow. The mean velocity, Reynolds stresses profiles, temperature and heat transfer rates obtained are compared with available experimental data. Reasonable agreement is obtained for the mean quantities.*

Keywords: *Impinging air jet, turbulence model, Nusselt number*

1. INTRODUCTION

Impinging jet is a very attractive and cost-effective technique because it can increase heat flux significantly near the stagnation point; and the wall heat transfer change noticeably if distance from the wall is small (Behnia *et al*., 1999). Therefore, impinging jets configurations are commonly used in numerous industrial applications such as drying of tissue, paper, textiles, and photographic films and cooling of high power density electronic components, because of their highly favorable heat and mass transfer characteristics.

The flow field of an impinging jet comprises three distinctive flow regions, namely a free jet region, a deflection region (or stagnation region) and a wall jet region. For high inlet-to-wall distances, the free jet region has three zones: the potential core zone, the developing zone and the fully developed zone (Viskanta, 1993). These regions are shown in Fig. (1). A shear layer is created due to the velocity difference between the potential core of the jet and the ambient fluid. Commonly this shear layer is the source of the turbulence in the jet; however, since in the present case, the inlet-to-wall distance is so short, there is not enough gap for mixing to happen with the surrounding fluid. As a result, the flow field in the vicinity of the stagnation point has low turbulence intensity. In the free jet region, the mean shear strain is zero and the production of kinetic energy is exclusively due to the normal straining. As the flow approaches the wall, the centerline velocity decreases to zero at the stagnation point. Moreover, the proximity of the solid boundary causes the deflection of the jet and a strong streamline curvature region is observed. Downstream the stagnation point, a wall jet evolves along the wall. Turbulence energy is increased due to the mean shear strain which dominates in the near-wall region.

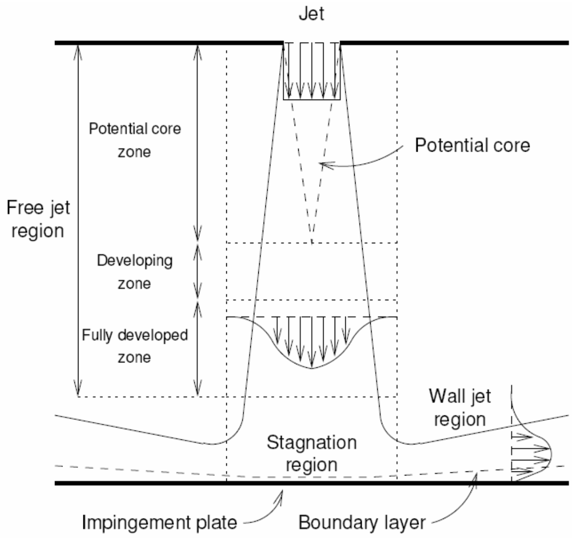

Figure 1. Flow regions of an axi-symmetric impinging jet.

Heat transfer rates in case of impinging jets are affected by various parameters like Reynolds number, nozzle-to-plate spacing (*H/D*), Prandtl number, target plate inclination, confinement of the jet, nozzle geometry, curvature of target plate, roughness of the target plate and turbulence intensity at the nozzle exit.

The axi-symmetric impinging jet is a challenging case for turbulence models validation as well as measurements techniques, due to the flow characteristics described. This is evidenced by the great number of publications concerning experimental, theoretical and numerical analysis for this configuration.

Martin (1977) and Downs & James (1987) presented a discussion on the influence of various parameters that control the heat transfer rate, such as the Reynolds number, nozzle-to-plate spacing and jet turbulent intensity.

Lytle and Webb (1994) have studied the effect of very small nozzle plate spacing ($H/D < 1$) on the local heat transfer distribution on a plate impinged by a circular air jet, by using an infrared thermal imaging system for temperature measurement. The velocity was measured by a Laser-Doppler Velocimetry (LDV) system. It was found that in the acceleration range of the nozzle plate spacing ($H/D < 0.25$), maximum Nusselt number shifts from the stagnation point to the point of secondary peak with the effect being more pronounced at higher Reynolds number.

A detail experiment study of impinging jet hydrodynamics, with information on the main turbulent characteristics was presented by Cooper et al. (1993), who made hot-wire measurements of a fully developed circular impinging jet for nozzle-to-plate spacing within the range of $2 \leq H/D \leq 10$ and Reynolds numbers within the range of $23{,}000 \leq \mathbf{Re} \leq 70{,}000$. Their results have been used for turbulence model assessment by, among others, Dianat *et al*. (1996) and Craft *et al*. (1993), who investigated the problem numerically, by employing a $\kappa-\omega$ eddy viscosity model. Very good predictions were obtained near the stagnation region of an impinging jet.

In 2002, Shi et al. studied the heat transfer of a turbulent jet flow, with several jet velocities and different nozzle-to-plate spacing (H/D). The $\kappa-\varepsilon$ and RSM models were employed, and it was concluded that both models slightly over predict the Nusselt number distribution, but the qualitative trends compared very well with the experimental data. Both models showed a significant influence in the Nusslet number distribution, due to the nozzle exit turbulence length scale, whereas the influence in the flow of turbulence intensity at the nozzle exit is more notable with the RSM model.

A Direct numerical simulation of turbulent heat transfer in plane due to an impinging jet was studied by Hattori & Nagano (2004). It was found from the DNS results that the Nusselt number increases with a decrease in the distance H, similar to the experimental data. In addition, it was concluded that for shorter distances, a second peak of the Nusselt number is observed away from the stagnation point, due to the increase in wall-normal turbulence intensities.

Hallqvist & Fuchs (2005) presented a study of the heat transfer of a turbulent swirling and non-swirling impinging jets, employing Large Eddy Simulation (LES). A nozzle-to-plate spacing $H/D = 2$ with Reynolds number of 23,800 and three Swirl numbers were considered. It was concluded that the production of turbulence increases with swirl, and promotes better wall heat transfer. Abrantes (2005) investigated experimentally the same phenomena, adopting two nozzle-to-plate spacing H/D=2 and 6. The Reynolds number was 21,000 and three Swirl numbers 0, 0.3 and 0.5 were considered. The results indicated that the circumferential components generate recirculation zones in the flow core, which significantly reduces the Nusselt number in the stagnation region.

In 2007, Hadziabdic & Hanjalic used a Large Eddy Simulation (LES), in order to gain a better insight into flow, vortical and turbulence structure and their correlation with the local heat transfer in impinging flows. A Reynolds number of 20,000 and the orifice-to-plate distance $H = 2D$ were defined. The periodic impact of large-scale eddies on the wall heat transfer is substantiated by the low level of stochastic turbulence and even negative production of the time-averaged turbulence kinetic energy around the stagnation point. Also in 2007, experimental studies were carried by Alekseenko *et al*. and Kim & Giovannini. Alekseenko *et al.* (2007) investigated the influence of different swirl rates, by employing a stereo PIV technique. The main emphasis of the work was the analysis of the influence of swirl rate on the flow structure. In their measurements, the Reynolds number was 8,900, the nozzle-to-plate distance was equal to three nozzle diameters and the swirl rate was varied from 0 to 1.0. It was found that the magnitude of pressure diffusion decreased with the growth of the swirl rate, and it was concluded that swirling impinging jets had a spread rate and a more rapid decay in absolute velocity when compared to the non-swirling jet. In the second paper Kim & Giovannini presented an experimental study of turbulent round jet flow impinging on a square cylinder laid on a flat plate. The jet from a long round pipe was 75 pipe diameters (D) in length, the Reynolds number was 23,000, and the square cylinder characteristics were ($3D \times 3D \times 43D$). Their measurements were performed using particle image velocimetry, flow visualization using fluorescent dye and infrared thermography. The turbulence statistics was investigated, the flow's topology observed, and it was shown a three-dimensional recirculation after separating from the square cylinder. A secondary peak in heat transfer coefficient was also observed, and its origin was attributed to very pronounced shear production coupled with the external turbulence coming from the free jet.

The present paper is part of on-going research regarding the flow characteristics of impinging jets. The objective of the present work is to evaluate the performance of the Reynolds Stress Model (RSM) in the characteristics prediction of the heat transfer process of an axisymmetric impinging jet on a plate, employing the commercial software Fluent, v.6.3. The mean velocity, Reynolds stresses profiles and heat transfer characteristics obtained are compared with available experimental and numerical data.

2. MATHEMATICAL MODELING

The Reynolds-averaged mass and momentum equations (RANS) were solved to determine the flow field. This approach is based on decomposing the velocity and temperature as $u_i = \overline{u_i} + u'_i$ and $T = \overline{T} + T'_i$, where $\overline{u_i}$ and $\overline{T}$ are the average velocity and temperature; u'_i and T' are the velocity and temperature fluctuation. The average continuity, momentum and energy equation for a steady and incompressible flow is given by

$$\frac{\partial \overline{u_j}}{\partial x_j} = 0$$

$$\frac{\partial}{\partial x_j}\left(\rho\, \overline{u_i}\, \overline{u_j}\right) = -\frac{\partial p}{\partial x_i} + \frac{\partial}{\partial x_j}\left[\mu \frac{\partial \overline{u_i}}{\partial x_j}\right] + \frac{\partial}{\partial x_j}\left(-\rho\, \overline{u_i'\, u_j'}\right) \tag{1}$$

$$\frac{\partial}{\partial x_j}\left(\rho\, \overline{u_j}\, \overline{T}\right) = \frac{\partial}{\partial x_j}\left[\frac{\mu}{\mathbf{Pr}} \frac{\partial \overline{T}}{\partial x_j}\right] + \frac{\partial}{\partial x_j}\left(-\rho\, \overline{u_j'\, T'}\right) \tag{2}$$

where ρ is the density, μ is the molecular viscosity, **Pr** is the Prandtl number, p is the pressure and x_i are the directions in the coordinate system. The momentum and energy equations presented have additional terms corresponding to the turbulent Reynolds stress term, $-\rho\, \overline{u_i'\, u_j'}$, and the turbulent heat flux $-\rho\, \overline{u_j'\, T'}$, representing the influence of the fluctuation on the average flow.

The Reynolds Stress Model, RSM (Gibson and Launder, 1978 and Launder *et al.* 1975) calculates all the components of the tensor $\overline{u_i' u_j'}$ using their transport equation. The computing effort of this model is much higher than the eddy viscosity models; however, it is capable of predicting turbulent anisotropy, unlike the former models. The RSM transport equation is obtained from the Navier Stokes equation and can be written as

$$\frac{\partial\, \rho\, \overline{u_k}\, \overline{u_i'\, u_j'}}{\partial\, x_k} = \frac{\partial}{\partial x_k}\left[\left(\mu + \frac{\mu_t}{\sigma_\kappa}\right)\frac{\partial\, \overline{u_i'\, u_j'}}{\partial\, x_k}\right] + P_{ij} + \Pi_{ij} - \frac{2}{3}\rho\, \varepsilon\, \delta_{ij}\ ;\ P_{ij} = -\rho\left(\overline{u_i'\, u_k'}\frac{\partial \overline{u_j}}{\partial x_k} + \overline{u_j'\, u_k'}\frac{\partial \overline{u_i}}{\partial x_k}\right) \tag{3}$$

In Eq. (4) the turbulent Prandtl number σ_κ is set as 0.82. P_{ij} is the stress production term and Π_{ij} the pressure strain term, based on low-Re Stress-Omega model (Wilcox, 1998) is given by:

$$\begin{aligned}\Pi_{ij} = &-(3.4\ \rho\ \varepsilon + 1.8\,P)\ b_{ij} + 4.2\ \rho\ \varepsilon(b_{il}\ b_{lj} - \frac{2}{3} b_{mn}\ b_{mn}\delta_{ij}) + (0.8 - 1.3\sqrt{b_{ij}\ b_{ij}})\rho\ \kappa\ S_{ij} + \\ &1.25\ \rho\ \kappa\,(b_{il}\ S_{kl} + b_{jl}\ S_{il} - \frac{2}{3} b_{mn}\ S_{mn}\delta_{ij}) + 0.4\rho\ \kappa\,(b_{il}\ \Omega_{jl} + b_{jl}\ \Omega_{il})\end{aligned} \tag{4}$$

where $P = (1/2)\, P_{kk}$. b_{ij} is the Reynolds-stress anisotropy tensor, S_{ij} and Ω_{ij} are the mean strain rate and mean rate-of-rotation tensor defined as

$$b_{ij} = -\left(\frac{-\rho\,\overline{u_i'\, u_j'} + (2/3)\rho\,\kappa\,\delta_{ij}}{2\,\rho\,\kappa}\right)\ ;\quad S_{ij} = \frac{1}{2}\left(\frac{\partial \overline{u_j}}{\partial x_i} + \frac{\partial \overline{u_i}}{\partial x_j}\right)\ ;\quad \Omega_{ij} = \frac{1}{2}\left(\frac{\partial \overline{u_j}}{\partial x_i} - \frac{\partial \overline{u_i}}{\partial x_j}\right) \tag{5}$$

The turbulent kinetic energy κ is obtained from the normal stress components, $\kappa = \overline{u_i'\, u_i'}/2$, and ε, the dissipation rate of κ, is determined by a similar ε equation of the standard κ–ε model

$$\frac{\partial\, \rho\, \overline{u_k}\ \varepsilon}{\partial\, x_k} = \frac{\partial}{\partial x_k}\left[\left(\mu + \frac{\mu_t}{\sigma_\varepsilon}\right)\frac{\partial \varepsilon}{\partial\, x_k}\right] + \frac{1.44}{2} P_{ii}\frac{\varepsilon}{\kappa} - 1.92\ \rho\ \frac{\varepsilon^2}{\kappa} \tag{6}$$

where σ_ε=1.0. The turbulent viscosity μ_t is also the same as the turbulent viscosity of the κ–ε model, $\mu_t = \rho\, C_\mu\, \kappa^2/\varepsilon$, where C_μ=0.09.

The turbulent heat flux $-\rho\, \overline{u_j'\, T'}$ is modeled using the Reynolds' analogy to turbulent momentum transfer as

$$\overline{\rho\ u_j'\ T'} = -\frac{\mu_t}{\mathbf{Pr}_t}\frac{\partial\ \overline{T}}{\partial x_k} \quad \text{with} \quad \text{Prt} = 0.85 \tag{7}$$

3. PROBLEM SETUP

The computational domain was defined based on the experimental apparatus of Abrantes (2005), with nozzle-to-plate spacing H/D=2, where D =13 mm is the diameter of the inlet jet The length in the radial direction was set equal to 13D. The origin of the Cartesian coordinate system is located at the stagnation point. As already mentioned, it was assumed symmetry in the angular direction; therefore, the problem was modeled as two-dimensional.

The Reynolds number based on the nozzle diameter, D, and average mean inlet jet velocity U_j

$$\mathbf{Re} = \rho\, U_j\, D\, /\, \mu \tag{8}$$

was defined as 21,000. The inlet axial values of velocity and inlet kinetic energy κ_{in} were obtained from the experimental LDV data of Abrantes (2005). The boundary conditions for the individual Reynolds stresses componets are derived from the turbulent kinetic energy, assuming isotropy of turbulence. The normal components are $\overline{u_i'\, u_i'} = (2/3)\,\kappa$ and $\overline{u_i'\, u_j'} = 0$. Non slip condition was imposed at the plate boundary, where a constant heat flux q_w is imposed. At the symmetry axis, zero gradients were specified to the axial velocity component and temperature, while the radial velocity is null. At all other boundaries, a pressure condition equal to 1 atm was considered, representing ambient far field condition, with the ambient temperature T_∞ equal to the mean jet temperature T_j.

The air properties were defined as: density and viscosity as 1.225 kg/m^3 and 1.7894 $\times 10^{-5}$ Ns/m^2, respectively. The thermal conductivity k and specific heat at constant pressure c_p were equal to 0.025 W/(mK) and 1006.43 J/(kg K), resulting in a Prandtl number **Pr**=0.72.

4. NUMERICAL METHOD

The flow field was numerically obtained with the commercial software *FLUENT*, v6.3, which is based on the Finite Volume method (Patankar, 1980). The ″QUICK″ scheme (Leonard, 1979) was used for the convective fluxes as this reduces the numerical diffusion, and the SIMPLE algorithm was employed to resolve the pressure-velocity coupling. The solution was considered converged when the sum of the normalized residuals of all equations was smaller than 10^{-6}.

A non uniform mesh, refined in the region closer to the centerline of the jet, and in the region near the impinging wall, with 24,000 control volumes was generated with the *FLUENT* auxiliary tool *GAMBIT*. A grid independent solution was assured by comparing results obtained with non uniform finer grids of 120,000 (300 × 400) and 187,500 (375 × 500) control volumes. It was observed differences between the solutions for the radial velocities inferior to 0.3%. The axial velocity profiles under the jet for these simulations were also in close agreement with each other.

The influence of the far field boundary condition was also investigated, and it was concluded that a larger computational domain was not necessary.

5. RESULTS

To evaluate the Reynolds Stress Model (RSM), initially the mean velocity and Reynolds stresses profiles are compared with available experimental data of Abrantes (2005), and with the predictions obtained with the κ−ω SST turbulence model by Maldonado e Nieckele (2008). Then, the temperature profile and Nusselt number prediction along the wall are examined.

Figure 2 presents a comparison of the normalized mean radial velocity v/U_j along the axial direction y/D, for several radial positions (r/D). To better visualize the results, the profiles are shown only near the flat plate. Away from it, the

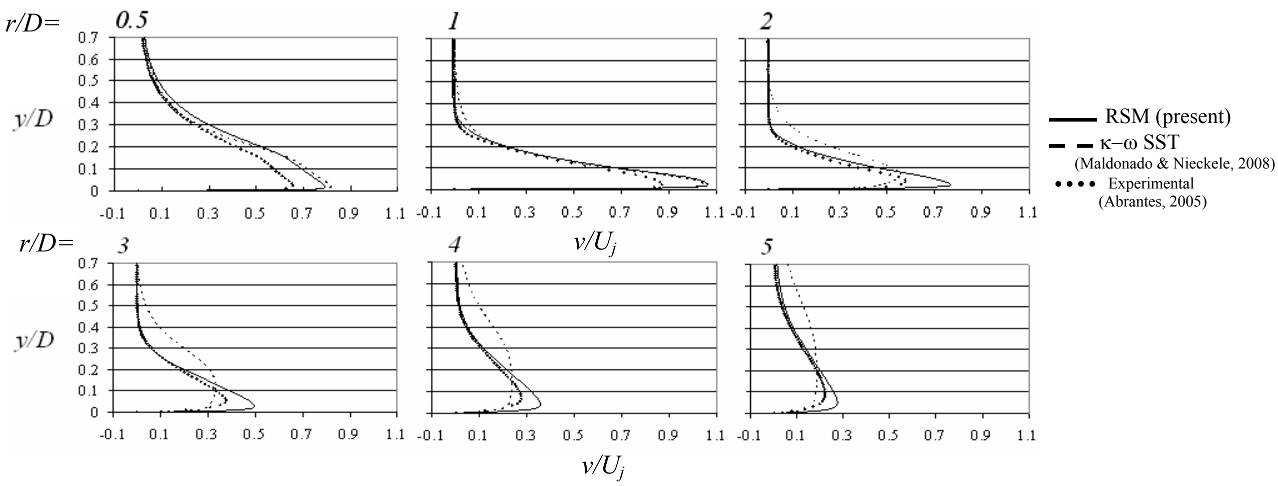

Figure 2. Mean radial velocity profiles.

agreement between the prediction and experimental data was very good. In can be seen that the prediction of the $\kappa-\omega$ SST model and RSM model show the same tendency as the experimental data. Near the stagnation point (r=0) the κ−ω SST e RSM models are quite similar and both overpredict the velocity. In this region (small r/D), an increase in the peak of the radial velocity near the plate can be observed, but as one moves away from the axis, the velocity peak rapidly decays. The velocity deceleration is stronger with the RSM model. Both models capture the strong velocity gradient in the region close to the plate wall. The uncertainty of experimental data in Abrantes (2005) for mean velocity was 1%.

Figure 3 presents the dimensionless mean radial velocity v^+ along the dimensionless axial direction y^+, for several radial positions (r/D), obtained with the RSM model. The experimental data of Abrantes (2005) is also shown. It can be seen the linear velocity ($u^+=y^+$) behavior near the wall ($y^+< 5$) and logarithmic relation between $5 < y^+< 10$ indicating the fully turbulent region. After that, there is a decay of the velocity to zero. It can also be seen that as the flows develops along the flat plate (larger r/D position) the flow becomes similar, since the curves tend to collapse.

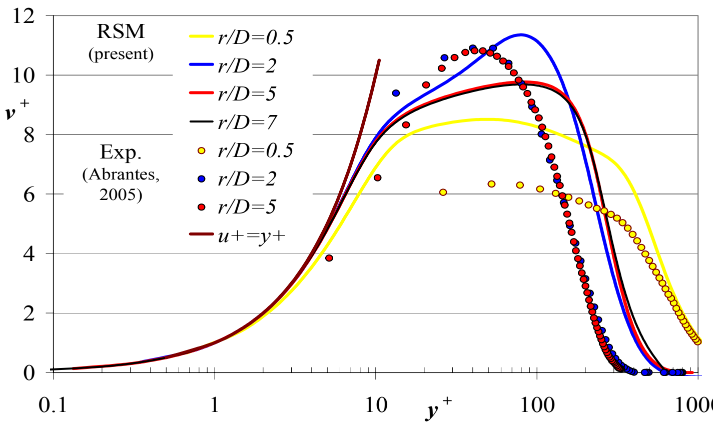

Figure 3. Mean velocity profile in wall units.

The Reynolds stress can be calculated from the solution of Eq. (3). The norms, rms of the turbulent fluctuations are:

$$\mathrm{rms}\,(u') = \sqrt{\overline{u'^2}} \qquad ; \qquad \mathrm{rms}\,(v') = \sqrt{\overline{v'^2}} \tag{9}$$

The norm rms of the radial and axial turbulent velocity fluctuation divided by the average inlet velocity U_j are presented in Figs. 4 and 5, at several radial positions. The uncertainty of experimental data provided in Abrantes (2005), for a turbulent radial and axial velocity was 2%. It can be seen in both figures, maximum values of the velocity fluctuations in the region close to the wall, because high levels of turbulence are presented in this region. It can also be seen, a sharp drop outside the wall jet region. Once again, both models are capable of capturing the main flow characteristics, however large discrepancies can be seen. The turbulent quantities are underpredicted by the κ−ω model, indicating that the model is too dissipative, while the RSM model prediction overestimated the peak values of turbulent axial and radial profiles. Larger spreading is also observed, indicating that the models are too dissipative.

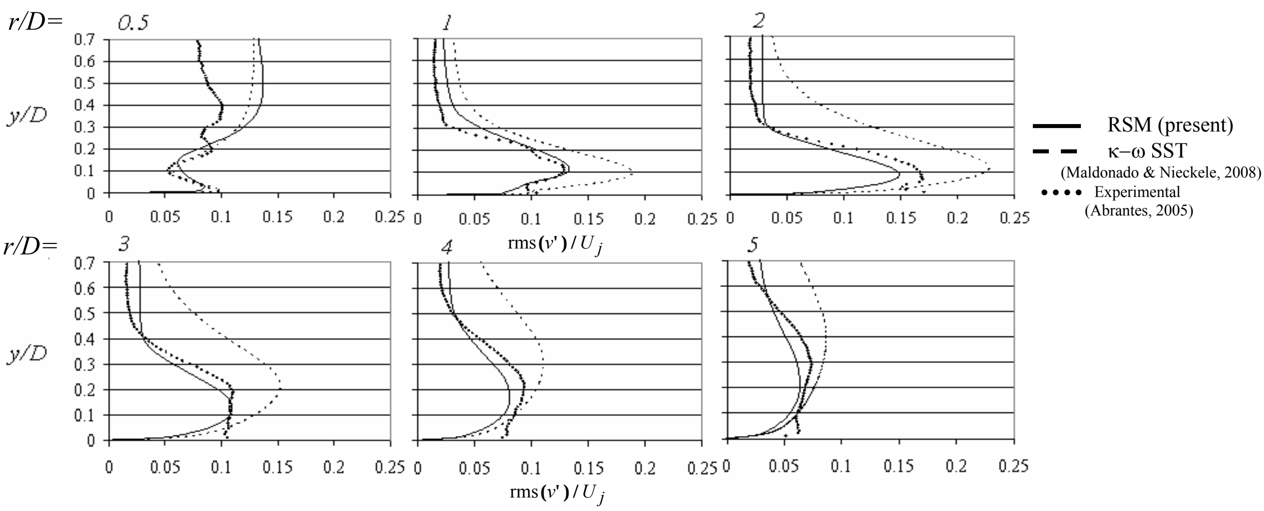

Figure 4. Turbulent radial velocity profiles. $\mathrm{rms}\,(v')/U_j$

Note that the experimental data showed smaller axial velocity fluctuations in relation to the radial fluctuations; however, the κ−ω SST and RSM models predicted approximately the same order of magnitude of both fluctuations. The turbulent intensity is diffused towards the jet axis, and therefore the position of peak values of the turbulent axial velocity shifts to the centerline as the axial distance from the jet axis grows. The discrepancies observed with the k-w STT model can be explained by the inability of the model to predict anisotropic turbulence. Although the RSM model claims to be able to predict turbulence anisotropy, the discrepancies observed can be explained by the lack of the third dimension in the simulations.

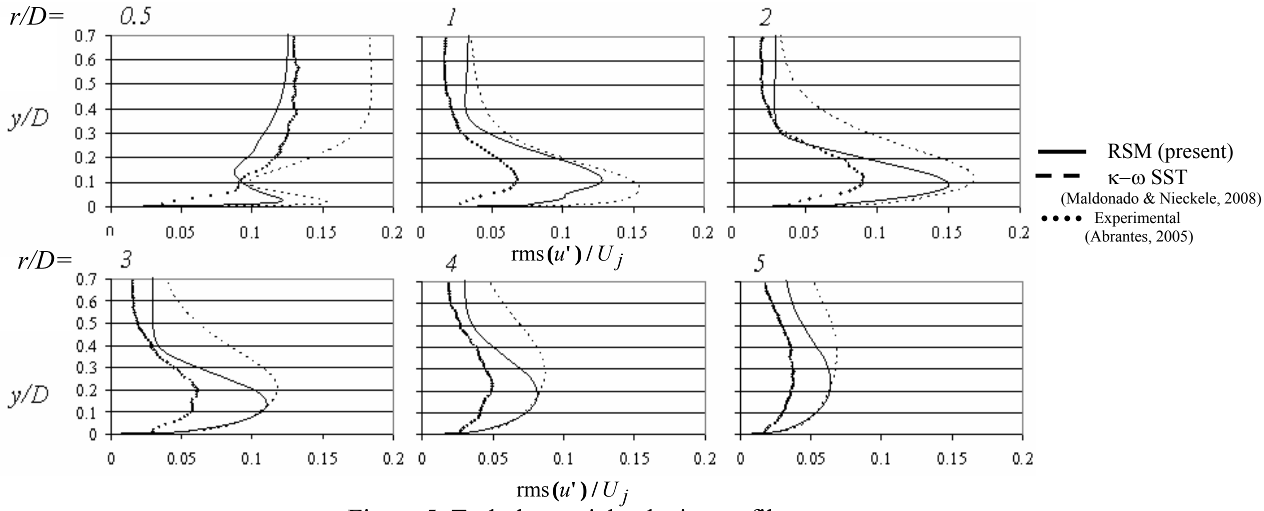

Figure 5. Turbulent axial velocity profiles. $\mathrm{rms}(u')/U_j$

The temperature distribution along the axial direction, obtained with the RSM model, is illustrated at Fig. 6, at various *r/D* positions. The jet temperature remains approximately constant until it reaches the plate and due to the imposed heat flux it rapidly increases. A thermal boundary layer can be observed along the plate, with the maximum heat transfer at the stagnation point (*r/D*=0). At the jet region *r/D* < 0.5, the temperature is approximately constant and equal to the jet temperature. As one moves away from the symmetry axis, due to the boundary layer formation along the plate, the air temperature increases, with higher values near the plate surface.

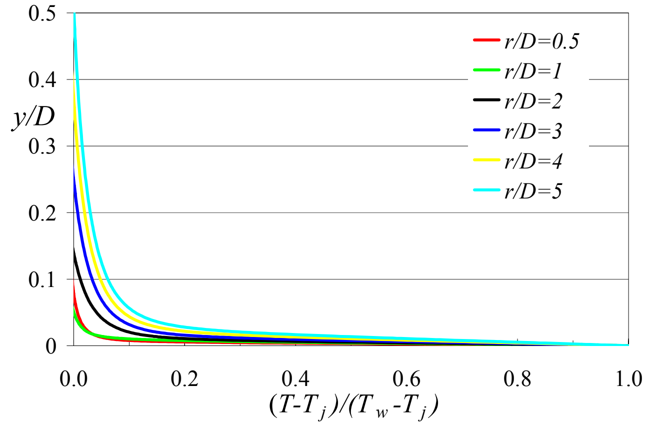

Figure 6. Temperature distribution along the axial direction at different *r/D* positions

The dimensionless temperature can be defined based on wall temperature T_w, wall heat flux q_w and friction velocity v^* as

$$\theta^+ = \frac{(T_w - T)}{\theta^*} \qquad \text{where} \qquad \theta^* = \frac{q_w}{\rho \, c_p \, v^*} \tag{10}$$

Figure 7a shows a distribution of mean temperature in wall unit, while in Figure 7b, the results of the direct numerical simulations (DNS) of Hirofumi and Nagano (2004) is presented. The mean temperature obtained at the present work with RSM for the coordinate *r/D*=2 presented excellent agreement with the numerical simulation (DNS) of Hirofumi and Nagano (2004). It can also be observed that for y^+ less than eight, the dimensionless temperature θ^+ varies linearly with the distance y^+ and it is proportional to **Pr**.

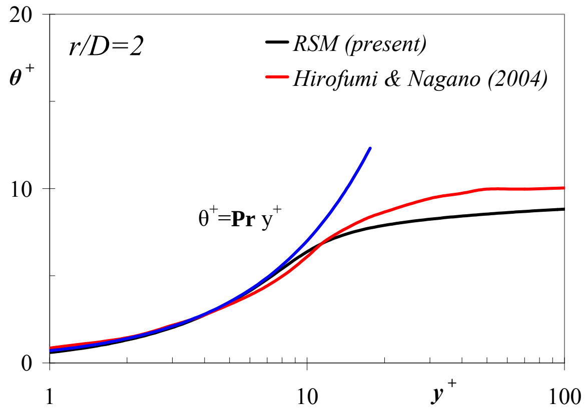

Figure 7. Distribution of mean temperature in wall unit

The Nusselt number is defined as

$$Nu = \frac{h\ D}{k} = \frac{q_w\ D}{(T_j - T_w)\ k} \qquad (11)$$

Figure 8 shows a comparison of the Nusselt number at the wall obtained in the present work with the RSM model with the experimental data of Abrantes (2005), *k-ω* SST model of Maldonado and Nieckele (2008) and the LES results of Hadziabdic, 2007). It can be observed that the LES results agreement with the experimental data are quite superior than both RANS models, which over-estimate the heat transfer at the stagnation region. It can also be seen that the RSM prediction is superior to the *k-ω* SST, which is unable to capture the secondary peak at r/D=2. This local maximum has been observed by a number of previous works of jet impinging on a wall, when jet-to-plate spacing is relatively small (H/D < 6), and its origin has been extensively discussed (Baughn and Shimizu, 1989; Kim & Giovannini, 2007). The secondary peak can be associated with the region where the turbulent kinetic energy reaches a maximum. Figure 9 presents the turbulent kinetic energy distribution near the plate surface, obtained with the RSM model, where it can be seen a peak of κ at $r/D \approx 2$ corresponding to the Nusselt number second peak.

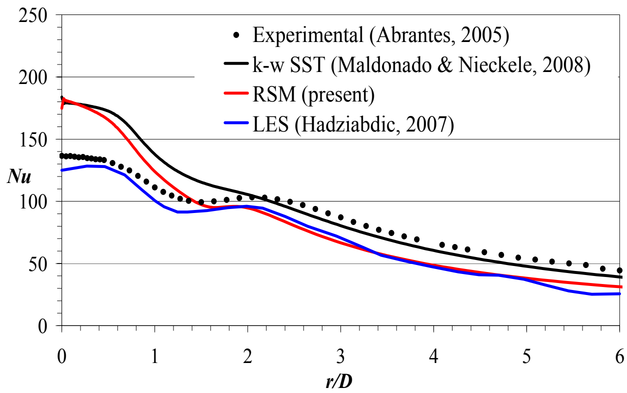

Figure 8. Nusselt number distribution

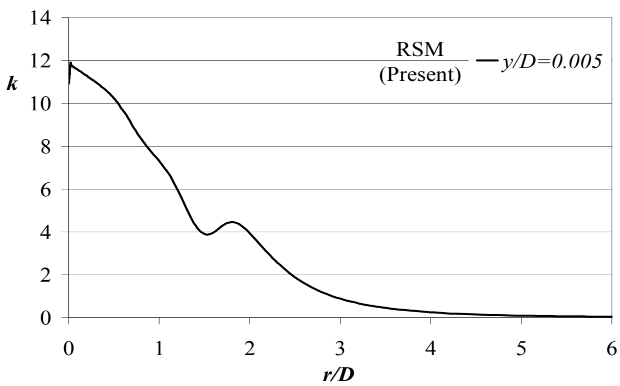

Figure 9. Turbulent kinetic energy at *y/D*=0.005.

6. CONCLUSIONS

In this work, the RSM was tested to evaluate its performance in the prediction of the heat transfer of an impinging jet. A comparison with experimental data showed some discrepancies, although the qualitative results were reasonable. The RSM overestimated the peak values of mean velocity radial, turbulent radial and axial velocity. The discrepancies can be attributed to the dissipation, leading to high levels of diffusion, especially in the axial momentum. The absence of the third component in the RSM modeling is also responsible for the discrepancies obtained.

It was observed that RSM overestimated a Nusselt number in the stagnation region. The occurrence of the second peak of the Nusselt number is associated with high levels turbulence kinetic energy, and it was reasonable predicted with RSM model, but no with *k-ω* SST model.

Although the RSM overestimated several variables, the qualitative behavior was reasonable. The results obtained with the RSM model were also similar *k-ω* SST predictions. Considering the reduced computational effort in relation to others simulations like LES or DNS, the quality of results can be considered acceptable, since the correct tendencies were predicted. Thus, in general terms, the RSM model presented reasonable results in terms of low computational effort and quality of results, compared with experimental data.

7. ACKNOWLEDGEMENTS

The authors gratefully acknowledge the support awarded to this research by the Brazilian Research Council – CNPq and CAPES.

8. REFERENCES

Abrantes, J.K., 2005, "Estudo do Escoamento e Transferência de Calor em um Jato Espiralado Incidente", Master's Thesis, in portuguese, Pontifícia Universidade Católica do Rio de Janeiro – PUC-RJ.

Alekseenko, S. V., Bilsky, A.V., Dulin, V. M. and Markovich, D. M., 2007, "Experimental Study of an Impinging Jet With Different Swirl Rates", International Journal of Heat and Fluid Flow, Vol. 28, No. 6, pp. 1340-1359.

Behnia, M., Parneix, S., Shabany, Y. and Durbin, P.A., 1999, "Numerical Study of Turbulent Heat Transfer in Confined and Unconfined Impinging Jets", Int. J. Heat Fluid Flow, Vol. 20, pp. 1-9.

Cooper, D., Jackson, D.C., Launder, B.E. and Liao, G.X., 1993, "Impinging Jet Studies for Turbulence Model Assessment-I. Flow-Field Experiments", Int. J. Heat Mass Transfer, Vol. 36, pp. 2675-2684.

Craft, T.J., Graham, L.J.W. and Launder, B.E., 1993, "Impinging Jet Studies for Turbulence Model Assessment-II. An Examination of the Performance of Four Turbulence Models", Int. J. Heat Mass Transfer, Vol. 36, pp. 2685-2697.

Dianat, M., Fairweather, M. and Jones, W.P., 1996, "Predictions of Axisymmetric and Two-Dimensional Impinging Turbulent Jets", Int. J. Heat Fluid Flow, Vol. 17, pp. 530-538.

Downs, S.J. and James, E.H., 1987, "Jet Impingement Heat Transfer – A Literature Survey", ASME, Paper no. 87 – HT-35.

Fluent Users Guide, 2008, Fluent Inc.

Gibson, M.M., Launder, B.E., 1978, "Ground Effects on Pressure Fluctuations in the Atmospheric Boundary Layer", J. Fluid Mech., Vol. 86, pp. 491-511.

Hadziabdic, M. and Hanjalic, K., 2007, "Vortical Structures and Heat Transfer in a Round Impinging Jet", Journal Of Fluid Mechanics, Vol. 596, pp. 221-260.

Hallqvist, T. and Fuchs, L., 2005, "Numerical study of swirling and non-swirling annular impinging jets with heat transfer", 35th AIAA Fluid Dynamics Conference and Exhibit, Toronto, Ontario, Canada, 6-9 June. pp. 1-14.

Hattori, H. and Nagano, Y., 2004, "Direct Numerical Simulation of Turbulent Heat Transfer in Plane Impinging Jet", International Journal of Heat and Fluid Flow, Vol. 25, No. 5, pp. 749-758.

Kim, N.S. and Giovannini, A., 2007, "Experimental study of turbulent round jet flow impinging on a square cylinder laid on a flat plate", International Journal of Heat and Fluid Flow, Vol. 28, No. 6, pp. 1327-1339.

Launder, B.E., Reece, G.J., and Rodi, W., 1975, "Progress in the Development of a Reynolds-Stress Turbulence Closure", Journal of Fluid Mech., Vol. 68(3), pp. 537-566.

Leonard, B.P. 1979, "A Stable Accurate Convective Modeling Procedure Based on Quadratic Upstream Interpolation", Computer Methods in Applied. Mechanics and Engineering, Vol.19, pp. 59-88.

Lytle, D., and Webb, B. W., 1994, "Air Jet Impinging Heat Transfer at Low Nozzle-Plate Spacings", Int. J. Heat and Mass Transfer, Vol. 37, pp. 1687-1697.

Maldonado, D.I. e Nieckele, A.O., 2008, Evaluation of the $\kappa-\omega$ SST Model For The Prediction of an Impinging Jet on a Plate, proceeding of V National Congress Of Mechanical Engineering ,Salvador, Bahia, Brazil, CON08-0824

Martin, H., 1977, "Heat and Mass Transfer between Impinging Gas Jets and Solid Surfaces", Advances in Heat Transfer, Academic Press, Inc., New York, E.E.U.U, Vol. 13, pp. 1-60.

Patankar, S. V., 1980, "Numerical Heat Transfer and Fluid Flow", Hemisphere Publishing, New York.

Shi, Y., Ray, M.B., and Mujumdar, A.S., 2002, "Computational Study of Impingement Heat Transfer Under a Turbulent Slot Jet", Industrial Engineering and Chemical Research, Vol. 41, pp. 4643–4651.

Viskanta, R., 1993, "Heat Transfer to Impinging Isothermal Gas and Flame Jets", Experimental Thermal Fluid Science Vol. 6, pp. 111–134.

Wilcox, D.C. 1998, "Turbulence Modeling for CFD", DCW Industries, Inc, La Canada, California

9. RESPONSIBILITY NOTICE

The authors are the only responsible for the printed material included in this paper.